Secondary Ice Formation during Freezing of Levitated Droplets

ANNIKA LAUBER,[a] ALEXEI KISELEV, THOMAS PANDER,[b] AND PATRICIA HANDMANN[c]

Atmospheric Aerosol Research, Institute for Meteorology and Climate Research, Karlsruhe Institute of Technology, Karlsruhe, Germany

THOMAS LEISNER

Atmospheric Aerosol Research, Institute for Meteorology and Climate Research, Karlsruhe Institute of Technology, Karlsruhe, and Institut für Umweltphysik, Universität Heidelberg, Heidelberg, Germany

(Manuscript received 23 February 2018, in final form 6 June 2018)

ABSTRACT

The formation of secondary ice in clouds, that is, ice particles that are created at temperatures above the limit for homogeneous freezing without the direct involvement of a heterogeneous ice nucleus, is one of the longest-standing puzzles in cloud physics. Here, we present comprehensive laboratory investigations on the formation of small ice particles upon the freezing of drizzle-sized cloud droplets levitated in an electrodynamic balance. Four different categories of secondary ice formation (bubble bursting, jetting, cracking, and breakup) could be detected, and their respective frequencies of occurrence as a function of temperature and droplet size are given. We find that bubble bursting occurs more often than droplet splitting. While we do not observe the shattering of droplets into many large fragments, we find that the average number of small secondary ice particles released during freezing is strongly dependent on droplet size and may well exceed unity for droplets larger than 300 μm in diameter. This leaves droplet fragmentation as an important secondary ice process effective at temperatures around −10°C in clouds where large drizzle droplets are present.

1. Introduction

Ice formation in mixed-phase clouds strongly affects their radiative properties and lifetime and controls precipitation initiation. At temperature higher than about −36°C, ice nucleating particles (INPs) are needed to initiate freezing of cloud droplets via heterogeneous ice nucleation. Yet field measurements in mixed-phase clouds have often detected a strong discrepancy between the observed number concentrations of cloud ice particles and INPs, the former being several orders of magnitude more abundant. The highest discrepancy is observed in marine clouds (e.g., Mossop 1985; Hobbs and Rangno 1985; Hogan et al. 2002; Crosier et al. 2011; Taylor et al. 2016). This discrepancy could only partly be explained by the shattering of ice particles on the instrument inlets (Knollenberg 1976; Korolev et al. 2011).

Various mechanisms have been suggested that are effective in increasing the total ice concentration by formation of more than one ice particle from a primary ice nucleation event, so-called secondary ice production (SIP) mechanisms: (i) mechanical fracturing of ice crystals upon collision (e.g., Vardiman 1978), (ii) ice crystal fragmentation caused by sublimation of dendrites (e.g., Oraltay and Hallett 1989), (iii) droplet splintering on freezing (e.g., Hobbs and Alkezweeny 1968; Johnson and Hallett 1968) and (iv) rime splintering (e.g., Hallett and Mossop 1974). Several SIP mechanisms can be active simultaneously or become active at different temperatures or on different stages of cloud evolution. Several model assessments were able to explain the discrepancy between INP and ice particle number concentration observed in clouds (e.g., Beheng 1987; Chisnell and Latham 1974;

Supplemental information related to this paper is available at the Journals Online website: https://doi.org/10.1175/JAS-D-18-0052.s1.

[a] Current affiliation: Institute for Atmospheric and Climate Science, ETH Zürich, Zurich, Switzerland.
[b] Current affiliation: Forschung Kältetechnik, Eckelmann AG, Mainz, Germany.
[c] Current affiliation: GEOMAR Helmholtz Center for Ocean Research, Kiel, Germany.

Corresponding author: Thomas Leisner, thomas.leisner@kit.edu

DOI: 10.1175/JAS-D-18-0052.1

Harris-Hobbs and Cooper 1987; Phillips et al. 2003; Rangno 2008; Sun et al. 2010; Vardiman 1978; Yano et al. 2016). However, the relative importance of the different SIP mechanisms and the corresponding production rates are not well understood (Field et al. 2017), and secondary ice formation remains one of the oldest unsolved mysteries in cloud physics. Small secondary ice particles can act as INPs at any temperature below 0°C themselves, and therefore, SIP may lead to an avalanche-type rapid glaciation of clouds.

In the range between about −3° and −8°C, the Hallett–Mossop (H-M) process is operative with a peak splinter production rate between −4° and −6°C; that is, ice particles grow through the collection of water droplets (riming) and might throw off secondary splinters during these collisions (Hallett and Mossop 1974). However, high secondary ice production was observed outside this temperature range (e.g., Rangno and Hobbs 1991, 1994, 2001; Stith et al. 2004). But even under favorable conditions, the H-M process alone might be too slow to explain observed rapid glaciation in clouds (Hobbs and Rangno 1990).

The mechanism of droplet fragmentation on freezing and secondary splinter ejection was revived recently upon the realization that this mechanism can be active outside the H-M temperature range (Kolomeychuk et al. 1975; Pander 2015; Takahashi 1975). It may trigger SIP in the colder parts of clouds, thereby supplying rapidly growing ice crystals into the lower, warmer H-M zone. Recent modeling work by Sullivan et al. (2018) has shown that droplet shattering can become an important mechanism of cloud glaciation for marine clouds, especially with warmer cloud bases and intermediate vertical updraft velocities.

Field observations imply that the presence of drizzle-sized drops enhances the efficiency of secondary ice production. In fact, large droplets were observed invariably before the occurrence of high ice particle concentrations began to appear (Braham 1964; Koenig 1963; Mossop 1970; Mossop et al. 1968, 1970, 1972).

To elucidate the mechanism of droplet fragmentation on freezing and ice splinter production, we have conducted a comprehensive series of laboratory experiments where secondary ice processes following the freezing of levitated water droplets have been identified and quantified using a high-speed video camera equipped with a microscope objective lens. This setup is described in some detail in section 2. In section 3, we present a classification of the observed SIP mechanisms and report their frequency of occurrence as a function of temperature, droplet size, and composition.

2. Experiment

Individual droplets were levitated in an electrodynamic balance (EDB) at temperatures between −5° and −30°C in particle-free air at a humidity corresponding to ice saturation. Freezing of the droplets was induced by contact with small (diameter $d < 10\,\mu$m) uncharged particles of ice that were introduced into the EDB. The process of freezing was observed by means of a high-speed video camera, and the resulting videos (see online supplemental material) were analyzed for identifying secondary ice processes occurring during or after freezing.

The EDB is a classical hyperbolic design consisting of a central electrode of an octagonal cross section and bottom and top endcap electrodes, which carry the ac and dc potentials needed for levitation (Hoffmann et al. 2013). The central electrode allows optical access through eight ports, which are used for the droplet position control system and the ultrafast video microscopy. A controllable flow of filtered air through the EDB in the vertical direction may be established to keep unwanted particles from entering the EDB. Droplets are generated by a piezoelectric dispenser (cf. below) and are introduced ballistically either via one of the horizontal ports or through an opening in the top electrode.

The droplet position in the EDB is controlled by a feedback loop. It is determined at a rate of 25 Hz by imaging light scattered from a diode laser beam onto a linear charge-coupled device (CCD) sensor vertically mounted outside the EDB. This position information is fed into a proportional–integral–derivative (PID) regulator that controls the dc potentials on the endcap electrodes. In a stagnant atmosphere, the dc voltage is used to infer the mass-to-charge ratio of the droplets, while changes in the dc voltage may be used to determine the droplet mass change due to evaporation and the gas velocity at the droplet position, as well as charge loss of the droplet.

The EDB is mounted inside a vacuum housing for thermal insulation. During the experiments, it is cooled by flowing ethanol from a thermostat through two channels in the central electrode. The temperatures of the center and endcap electrodes are monitored individually. The droplet temperature is calculated by a weighted average of the electrode temperatures. The weighting coefficients are determined beforehand by inserting a tiny resistance temperature sensor into the EDB at the droplet position. If (typically at higher temperatures) the droplets evaporate substantially during the period of observation, evaporative cooling is estimated from their size change, and the droplet temperature is corrected accordingly. The absolute droplet temperature may also be influenced by the gas flow around the droplet and is estimated to be accurate within ±0.6°C.

The bright-field images of the droplets are recorded by the high-speed video camera (Phantom v710, Vision

Research) equipped with a 10-times long working distance microscope objective (Mitutoyo). The droplets are illuminated by a white light-emitting diode (LED) mounted opposite to the camera objective. Video frames with an exposure of 10 μs were typically recorded at a rate of 20 000 frames per second.

Droplets of two different sizes have been studied in our experiments. Droplets with a diameter of approximately 85 μm (small droplets) were generated with a piezoelectric drop-on-demand dispenser (model SPIP, GeSim) and injected laterally through one of the ports in the central electrode. Droplets with a diameter of 310 μm (large droplets) were generated with a piezoelectric dispenser (PipeJet P9 Nanodispenser, BioFluidix). This dispenser was installed on the top of the EDB, and the droplets were injected vertically through an axial opening in the top electrode. To decelerate and trap large droplets, the dc voltage between the endcap electrodes was pulsed to a high value (typically 800 V) during injection. In both cases, droplets were charged by induction from an electric field at the dispenser tip created by an external electrode. By varying the voltage at this electrode, the polarity and amount of charge on the droplets could be varied (Rzesanke et al. 2012). Over a period of several years, about 8000 freezing events of small droplets and about 800 freezing events of large droplets have been recorded. The charge on the small droplets was varied between +1 and +2.5 pC; the large droplets carried charges ranging between +8 and +14 pC.

Experiments with pure water, artificial sea salt solutions, and polystyrene latex (PSL) bead suspensions were conducted. We have used either NANOpure water (Barnstead-Thermolyne; 18 MΩ cm^{-1}) or CHROMALOV-Plus water (Sigma-Aldrich) to prepare pure water droplets or suspensions. PSL suspensions were prepared by diluting commercial PSL suspensions (diameter ≈ 400 nm; Z-PS-POS-000-0.4, Postnova) with NANOpure water. For both droplet sizes, the particle concentration was around 100 particles per droplet. Sodium chloride solutions were prepared by dissolving either NaCl or Instant Ocean (Spectrum Brands), a mixture of inorganic sea salts, in NANOpure water. Concentrations were varied between 2 and 0.1 g L^{-1}, reflecting typical concentrations of sea salt aerosol in cloud water (Turner 1955).

The video recordings of freezing events were analyzed by standard image analysis techniques provided within the LabVIEW (National Instruments) image analysis package. The parameters analyzed routinely for each video frame were the size and position of the droplet and the area, length, and direction of protrusions from the droplet. This automated analysis was used to detect fragmentation events, as they are often associated with a shift in droplet position due to a charge loss, recoil momentum, or change in aerodynamic drag. In cases where one or more ejected particles could be detected on the video recording, their speed was determined by the length of the streak they formed on the video frame (cf. Fig. 1, red circle).

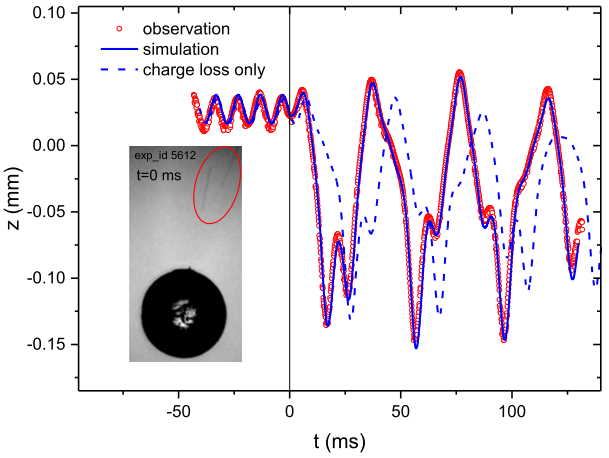

FIG. 1. Observed (circles) and modeled (solid line) vertical displacement of a levitated freezing droplet during a secondary ice event. The video image corresponding to time $t = 0$ is shown in the insert; the two ejected fragments are marked by the ellipse. The only two fitting parameters were the charge loss and the vertical component of the recoil momentum; the latter was set to zero to obtain the dashed line.

Assuming that the detected fragments are the only particles ejected from the parent droplet, their mass can be obtained from momentum conservation. As the motion of the parent droplet is influenced not only by recoil but also by charge loss, the trajectory of the parent particle needs to be analyzed with the help of numerical simulations. We obtain the electrical field components in the geometry of our EDB with the help of the SIMION ion optics simulation program (Scientific Instrument Services, Inc.) and integrate the equations of motion of the droplet and the fragments, taking into account electrical forces in the trap field, Coulomb repulsion between particles, and friction forces in the surrounding gas. An example of such an analysis is shown in Fig. 1. The z coordinate of an observed particle trajectory during a secondary ice ejection is compared to a simulation with fitted charge loss and recoil momentum as the only free parameters, with all other parameters determined from measurements. For comparison, the simulation of a droplet trajectory that accounts for charge loss only without recoil is given as the dashed line. Obviously, this type of analysis is able to reproduce the observed trajectories and under favorable conditions allows determining charge loss and recoil momentum during a fragmentation event.

Electrodynamic levitation employs electric fields that are at the droplet position comparable in magnitude to natural electric fields encountered in clouds (several kilovolts per meter; Dye et al. 1989) but requires the droplets to be electrically charged beyond levels typically encountered in clouds, which range between virtually zero in shallow clouds and several picocoulombs in highly electrified clouds (MacGorman 1998). We argue here that this charge does not change the dynamics of the mechanical breakup of freezing droplets, which occurs (cf. below) when the freezing process is nearly complete. The forces exerted by the surface charges on the ice shell translate into a negative pressure of at most 0.005 MPa for a drop of 300-μm diameter charged to 10 pC. This is several orders of magnitude below the tensile strength of ice, which varies between 0.7 and 3.1 MPa (Petrovic 2003). However, the droplet charge does attract small electrically polarizable ice crystals from the surrounding, thus facilitating the initiation of freezing in our experiment.

3. Results

Droplet freezing is a two-step process (Pruppacher and Klett 1997). After nucleation, ice grows in a dendritic fashion throughout the droplet until the latent heat released by crystallization has raised the droplet temperature to the melting point. From then on, the latent heat of fusion has to be transferred to the surrounding atmosphere via heat diffusion and evaporation from the surface, leading to an ice shell growing outside in and surrounding a slushy water–ice core. All SIP processes reported below were observed during that second stage of freezing. As the specific volume of ice is larger than that of water, the growth of the ice shell induces a high pressure on the slushy core, which may lead to a remelting of that part of the droplet. As the ice grows, gasses dissolved in the water are rejected from the crystal lattice of ice and concentrate in the shrinking liquid phase. The high pressure within the droplet hinders the nucleation of the dissolved gasses into bubbles. As the ice shell grows, the pressure inside the freezing droplet increases, imposing a strong mechanical stress on the ice shell. This mechanical stress can be released by slow processes like plastic deformation of ice shell or percolation of water through cracks in the shell followed by droplet deformation or by more violent processes that lead to the ejection of secondary ice particles. We summarize the latter as SIP mechanisms and classify them into two main categories: splitting and ejection. Splitting involves the cracking of the droplet around its perimeter and may result in the formation of two or more large ice fragments, while in the ''ejection'' case, small ice fragments are ejected locally, and the parent particle stays largely intact. In the following section, we qualitatively describe these two categories, introduce subcategories, and give estimates of their relative frequencies of occurrence as a function of droplet size, temperature, and composition. The following discussion concentrates chiefly on large droplets, where SIP events were much more frequent. We first classify and describe the observed SIP mechanisms and later quantify them.

a. Ice ejections

1) BUBBLE BURSTING

Gas bubble formation on the surface of a droplet and their subsequent bursting has been observed quite frequently in this study. At temperatures around −6°C, about 75% of the large droplets and about 6% of the small droplets at around −11°C produced small bubbles on their surface during freezing, with an estimated average of about 16 and 5 bubbles per large and small droplet, respectively. Most of these bubbles did eventually burst, ejecting fragments of the bubble skin. In some cases, this was accompanied by a charge loss and detectable recoil. Bubbles formed predominantly at the tip of a spicule (see Fig. 2) but also at the droplet surface. These two cases are discussed separately below.

Once a small crack opens in the ice shell, the dissolved gasses and water will be pushed out of the droplet. Upon exiting the crack, water will freeze on its rim in form of a ring through which more water is expelled, thus building up a spicule. The appearance and growth of these spicules have been described frequently in the literature (e.g., Pander 2015; Wildeman et al. 2017). When the pressure within the bulk of the droplet is relieved, dissolved gasses may nucleate into bubbles, which are expelled through the spicule and reside at its tip. Here, they are exposed to the colder environment outside the drop, which itself has warmed to 0°C and burst at the latest by the time they freeze. Subsequently, more water and more bubbles may follow the same channel, leading to a repetition of this process. If the bubble film was frozen at the time of bursting, ice particles are released and would grow via vapor deposition in the water-saturated environment.

On average, 2.4 bubble-bursting events on an individual spicule could be observed, with 12 events being the highest number. Here, only bursting bubbles that released at least one optically detectable larger ice fragment or that lead to a detectable recoil of the parent droplet were counted. An example of two subsequent bubble bursts occurring at one spicule is shown in Fig. 2.

Bubbles may also form directly on the surface of freezing droplets without a spicule being grown beforehand.

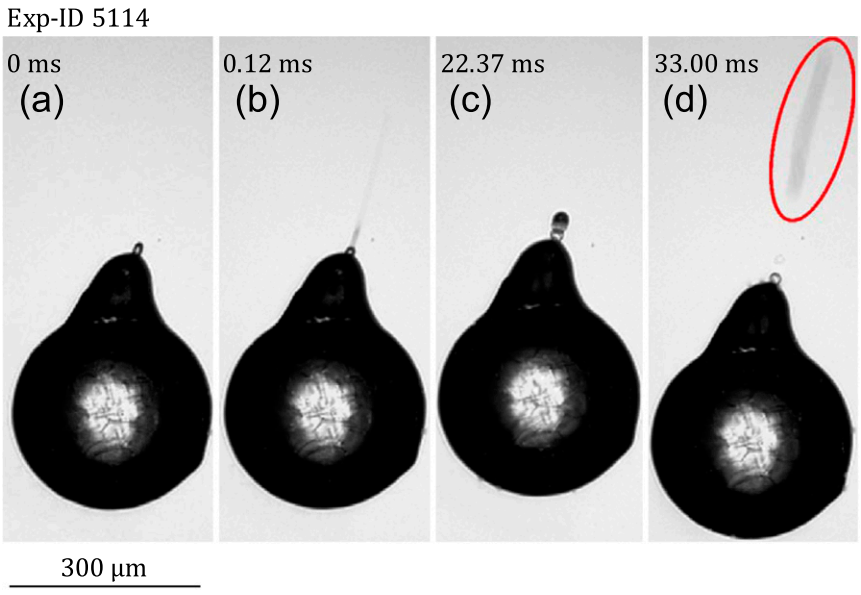

FIG. 2. Sequence of video frames showing two spicule bubble-bursting events: (a) a spicule formed on a bulge; (b) the tip of the spicule bursts; (c) a new bubble has formed at the spicule tip; and (d) the newly formed bubble bursts. Times are given relative to the time of (a). Streaks of emitted particles are marked by red ellipses.

In these cases, they appear at cracks that form in the ice shell as a result of the pressure rise inside the freezing droplet. Surface bubbles are observed mainly toward the end of the freezing process when almost all liquid water is frozen and all of the dissolved gasses have nucleated into bubbles, as then there is not enough liquid water left for spicule formation. Again, surface bubbles will burst at the latest once they freeze, and fragments of the bubble film might contribute to secondary ice particle formation. An image sequence of the bursting of a particularly large bubble with visible fragments is shown in Fig. 3. In general, surface bubbles only rarely lead to visible fragments or detectable recoils, as they often burst without any observable change in the droplet position. For large droplets, not more than two surface bubble-bursting events accompanied by a detectable recoil momentum were observed with an average occurrence rate of 1.1. Surface bubbles bursting without detectable recoil or charge loss were observed more frequently but are not classified as secondary ice events here as we do not know the phase of the ejected particle.

2) JETTING

Without any spicule or bubble growing, a sudden liquid jet from the droplet surface was observed occasionally. Such jets last just for about 100 μs, so they are not temporarily resolved on the video recordings. It is not clear if the jet is only liquid water or if it carries small pieces of ice with it. Only in the latter case can it be classified as SIP event. All jetting events led to strong recoils of the parent droplet and must therefore be accompanied by a considerable mass loss. One example of jetting is shown in Fig. 4. We report below the frequency of occurrence of jets, but an average number of ejected particles per jet cannot be determined.

b. Splitting

Large cracks extending across the whole diameter of the droplet appear when the pressure inside the droplet exceeds the threshold of mechanical stability of the ice shell. The ice shell then splits into two parts of roughly equal size. This process is termed splitting here and is divided into two categories: cracking and breakup, with respective subclasses.

1) CRACKING

During many splitting events, the capillary force exerted by the liquid core within the droplet is able to keep the two pieces of the ice shell together after the crack opened and the internal pressure is released. We term this process ''cracking'' when the two halves seal together in almost their original position and orientation and the cracks are hardly visible afterward. An example of such a process is given in Fig. 5. Often, a bubble of external air is taken up into the interior during the negative pressure phase following the crack. Only in one

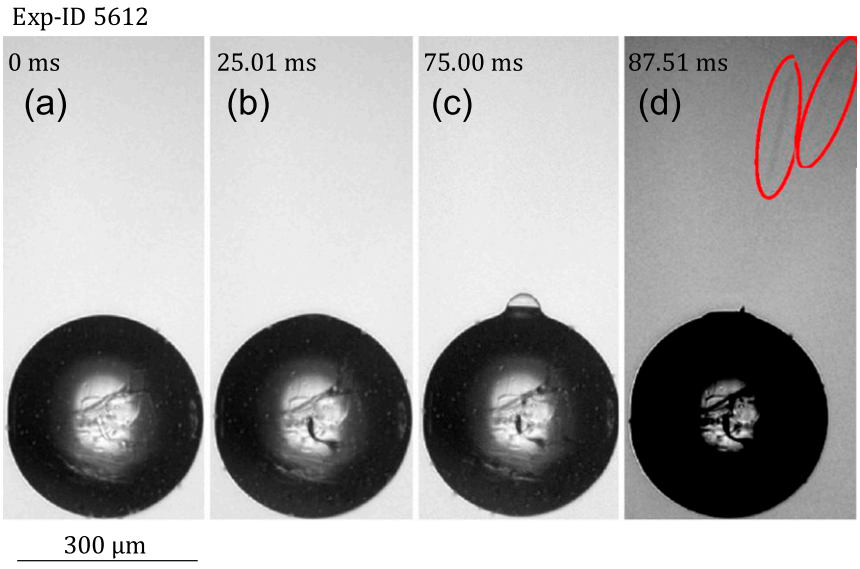

FIG. 3. Sequence of video frames showing a bubble bursting on the surface of a frozen large droplet: (a) a droplet near the end of its freezing process with small cracks visible near the center; (b) water and dissolved gasses are percolating through a crack; (c) a large bubble has grown on the surface; and (d) the bubble bursts and two pieces of the ejected shell can be seen at the top right corner (red ellipses). The time is given relative to (a). [In (d), the brightness mapping has been adapted for better visibility of the ejected particles.]

case, which is depicted in Fig. 5, could the ejection of a particle or a small droplet be observed during such a process. Nevertheless, it cannot be excluded that cracking is accompanied by the emission of smaller ice particles like those reported by Kolomeychuk et al. (1975), being either splinters from the cracking process itself or being shaken off mechanically from the surface during the rapid motion. Below, we report the frequency of

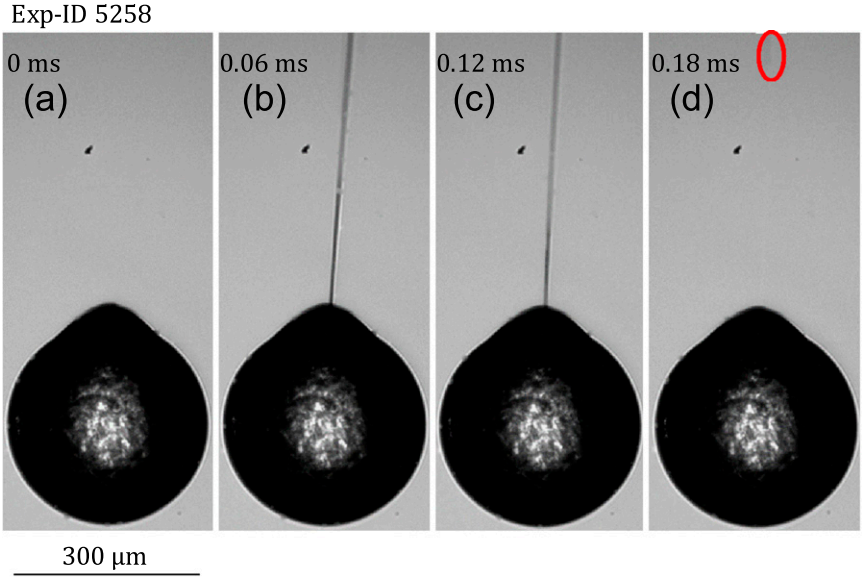

FIG. 4. Sequence of video frames showing jetting: (a) a droplet just before the jetting event; (b),(c) extended jet clearly visible; and (d) jetting has stopped; jet tail is marked at the top of the picture. Time is relative to (a). The dark spot in the upper half of the panels is a particle on the complementary metal–oxide–semiconductor (CMOS) camera sensor.

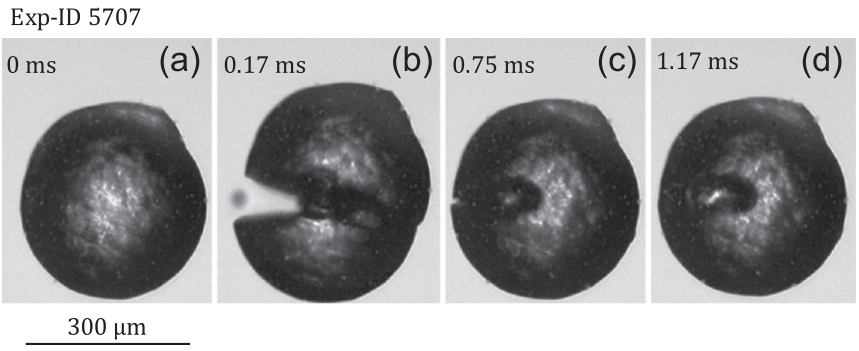

FIG. 5. Sequence of video frames showing the breakup and closure of a freezing droplet, here called cracking: (a) freezing droplet just before the event; (b) a crack opens across the droplet and a small particle or droplet is ejected; (c) the crack closes again and a large gas bubble is taken up by the droplet; and (d) the crack has completely sealed and only the bubble inside the droplet remains visible. Time is relative to (a).

cracks without assigning an average number of ejected particles.

2) BREAKUP

The breakup of a freezing droplet into two almost hemispherical fragments has been reported in the literature and is often referred to as shattering (e.g., Knight and Knight 1974; Takahashi 1975) or fragmentation (e.g., Pander 2015). We hesitate to call this shattering, as this is often used to describe the disintegration into multiple fragments [like in the processes described in Wildeman et al. (2017)]. Freezing droplets break apart when the cracking is energetic enough to overcome the negative pressure and the capillary forces that try to hold the two halves together. Sometimes, small particles or droplets are also ejected during a breakup, an example being shown in Fig. 6. Occasionally, a water bridge between the two halves holds the droplet fragments together so that the breakup event is not completed. Such an "incomplete breakup" can also lead to SIP when small ice particles are ejected during the breakup or because of its new unstable shape, which can easily break at the next collision.

c. Frequencies of SIP occurrence

For small ($d \sim 85\,\mu$m) droplets, we observe SIP only for droplets containing solid inclusions. In the observations of freezing of 1000 individual pure water droplets, only five ice production events have been detected in the temperature range between −5° and −30°C. For PSL suspension droplets, we found an occurrence frequency of SIP that was about 50 times higher but surprisingly did not depend on the concentration of the PSL particles in the droplet. We observed SIP at a PSL concentration of less than 10 PSL particles per droplet but report here the data for a concentration of about 100 particles per

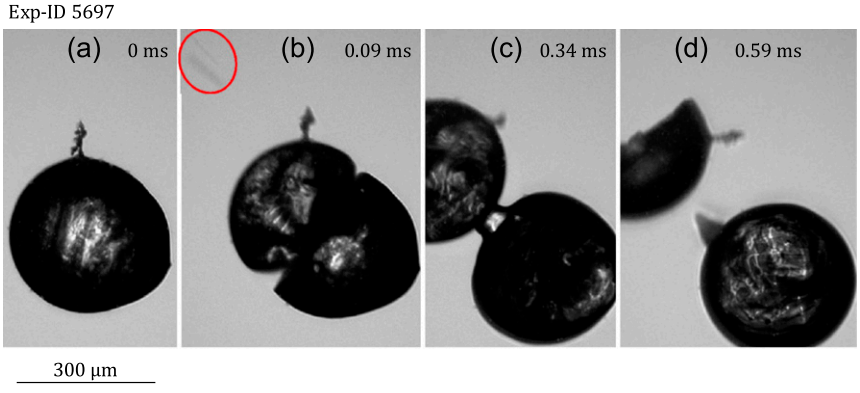

FIG. 6. Sequence of video frames showing a breakup of a freezing droplet: (a) a droplet just before the event; (b) a crack opens and two ejected particles can be seen at the top left corner (red ellipses); (c) the two fragments are held together by a water bridge; and (d) the bridge breaks and the two pieces are separated. Time is relative to (a).

droplet, where we have the largest dataset. Figure 7 shows the relative frequency of occurrence of SIP for small droplets of a PSL solution, both for ejection and breakup processes (cracking events were not analyzed). The overall frequency reaches a maximum of roughly 10% between about −10° and −20°C. Note that the breakup frequency maximum is shifted toward lower temperature compared to the ejection events, which are most frequent near −10°C.

For large ($d \sim 310\,\mu$m) droplets of pure water, we find a much more frequent and more diverse occurrence of SIP. The SIP frequency is increased even further by the presence of solid inclusions. Figure 8 shows quantitatively our results both for pure and for PSL-containing large water droplets. As evident from Fig. 8, more categories of SIP mechanisms have been identified for the large droplets. Ejections have been divided into jetting, surface bubble bursting, spicule bubble bursting, and "unidentified" ejection type. "Splitting" has been divided into "breakup" and "cracking," the latter not included in the results of the small droplets. For the pure water droplets, the total SIP frequency reaches up to 35% and peaks at a temperature around −10°C. PSL-containing droplets reach up to 75% at a similar temperature, with the splitting processes being strongly enhanced. The SIP frequency peaks at higher temperatures compared to the small droplets. An additional ejection type subcategory "unidentified" was added for the recoils that were observed without ejections or where the observed ejection could not be clearly assigned to one of the above classes, mostly because the frame rate was too low. Most likely, they can be attributed to bubble-bursting or jetting events. Our results for large droplets are summarized in Table 1, giving the maximum occurrence frequencies and the respective temperature intervals for the SIP mechanisms. Table 1 also reports the average number of secondary ice particles per freezing droplet detected for each of the SIP mechanisms.

We have also investigated the freezing of sea salt solution droplets and found that high concentrations of sea salt effectively suppress all secondary ice processes for both size classes. At salt concentrations above 2000 mg L^{-1}, none of the observed droplets showed recoil or splitting events. In contrast to the pure or suspension droplets, all droplets stayed spherical during the freezing process. Only after the salt concentration was reduced to 100 mg L^{-1} (0.7-μm salt particle dissolved in 20-μm water droplet) has secondary ice formation been observed again. For this concentration, surface and spicule bubble bursting were observed in a temperature range between −18° and −6°C with the occurrence frequency of about 10%.

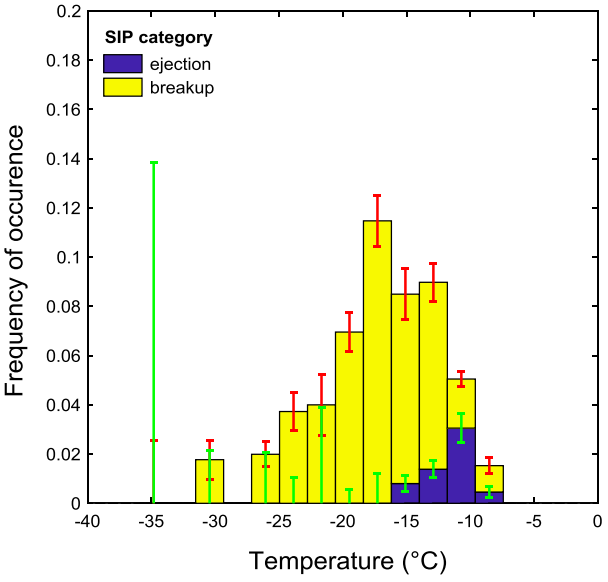

FIG. 7. Mechanism-resolved SIP frequency of occurrence for small water droplets mixed with PSL particles as a function of temperature.

4. Discussion

The main limitation of this work is our inability to detect subvisible fragments smaller than about 2 μm in diameter. Furthermore, the particle phase (liquid or solid) could not be identified reliably in bubble-bursting and jetting events. These factors impose an unknown uncertainty on our estimate of secondary ice particles produced in a secondary ice process, and the numbers we report here have to be considered as lower limiting values. Minor uncertainties arise from the limited duration and frame rate of the individual video recordings. The missing third dimension perpendicular to the field of view of the camera is of minor importance, as most ice multiplication events can be detected by charge loss even if not observed visually. Moreover, freezing droplets tend to orient in the EDB with their longest axis in vertical direction. Since the majority of ejection events takes place from extremities (e.g., spicule bubble bursting), and splitting can be observed from any perspective, the majority of secondary ice particle production events could be detected.

Small drops ($d \sim 85\,\mu$m) of NANOpure water did not show SIP in our experiments. In the presence of solid inclusions (PSL), only 10% of all small freezing droplets would produce secondary ice particles at comparatively low temperatures. It suggests that SIP upon freezing is a strong function of droplet diameter. We speculate that the solid inclusions can reduce the mechanical stability of the ice shell and may act as nucleation sites for cracks.

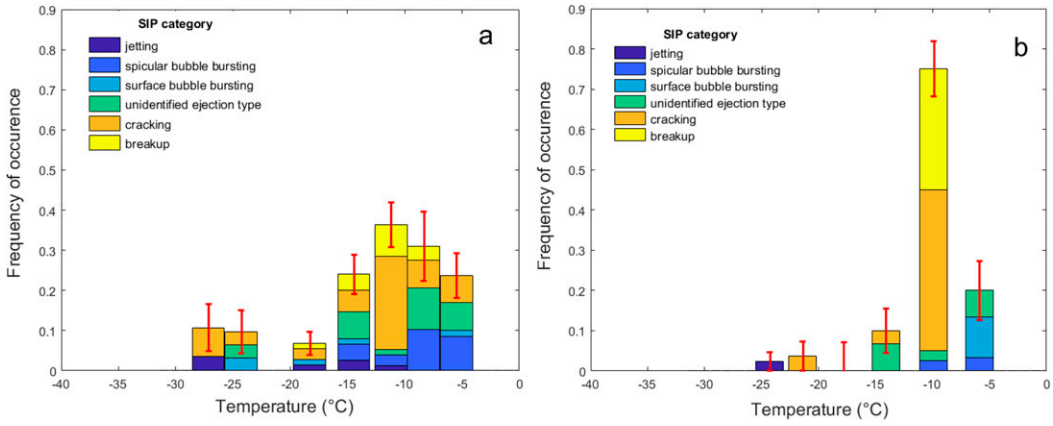

FIG. 8. Mechanism-resolved SIP frequency of occurrence for large droplets as a function of temperature: (a) pure water droplets and (b) droplets containing PSL particles.

The maximum occurrence frequencies and the respective temperature intervals for the SIP are summarized in Table 1. It also reports the average number of secondary ice particles detected for each of the SIP categories. Secondary ice particles might have been missed in our analysis if they are too small to be detected optically, if they are emitted in the time interval between two video frames, or if they are ejected in a direction out of the focal plane of the microscope objective lens. Therefore, the average number of observed secondary particles could considerably underestimate the real number of secondary ice particles emitted.

As evident from the higher frequency of occurrence and the higher number of secondary particles per event, ejection processes dominate over splitting processes. The former also occur at higher temperatures. We reason that at higher temperatures, the ice shell around the freezing droplet is less rigid, allowing for an effective pressure reduction and leading to a suppression of splitting processes. The latter is only effective at colder temperatures, where ejections are much less frequent. In the temperature interval between −10° and −6°C, bubble bursting may be responsible for more than one secondary ice particle per freezing droplet.

A comparison of our results to previous work on droplet shattering upon freezing is hampered by the various experimental approaches used in the past and the varying nomenclature in the literature. The droplet size dependence of SIP was discussed by Kolomeychuk et al. (1975), who reviewed experiments on freely suspended droplets, legitimately arguing that a support would influence the freezing behavior of droplets (Johnson and Hallett 1968). The summary of their data complemented by our results is given in Fig. 9. It shows a clear increase in overall fragmentation frequency and in the number of ejected secondary ice particles per fragmenting droplet with increasing droplet size. The latter seems to be more pronounced, as we observe a maximum of 12 secondary splinters from a droplet size of 310 μm compared to a maximum 142 splinters observed for the 1.6-mm large droplets. It should be noted, however, that the detection limits have been different, and the results are not fully comparable.

As cloud droplets often nucleate on soluble aerosols, the effect of salt on SIP was addressed. In agreement

TABLE 1. Description of the SIP categories, their maximum occurrence frequencies for large droplets, and an estimate of the number of secondary ice particles produced in a freezing event. The occurrence frequency includes only the ratio of droplets that underwent the specified process and does not account for multiple ejections per freezing event.

SIP mechanism	Category	Subcategory	Frequency of occurrence max value	Temperature interval of highest occurrence	No. of secondary particles per freezing event
Ejection	Bubble bursting	From spicule	10.3% (±5.7%)	−10° to −6°C	>2.4
		From surface	10.0% (±5.5%)	>−10°C	>1.1
	Jetting	—	3.6% (±3.5%)	<−25°C	Unknown
	Unidentified	—	10.3%	−10° to −6°C	Unknown
Splitting	Cracking	—	40.0% (±7.7%)	−14° to −6°C	Unknown
	Breakup	Complete	27.5% (±7.1%)	−14° to −6°C	>2.4
		Incomplete	4.9% (±2.8%)	−13° to −9°C	>0.1

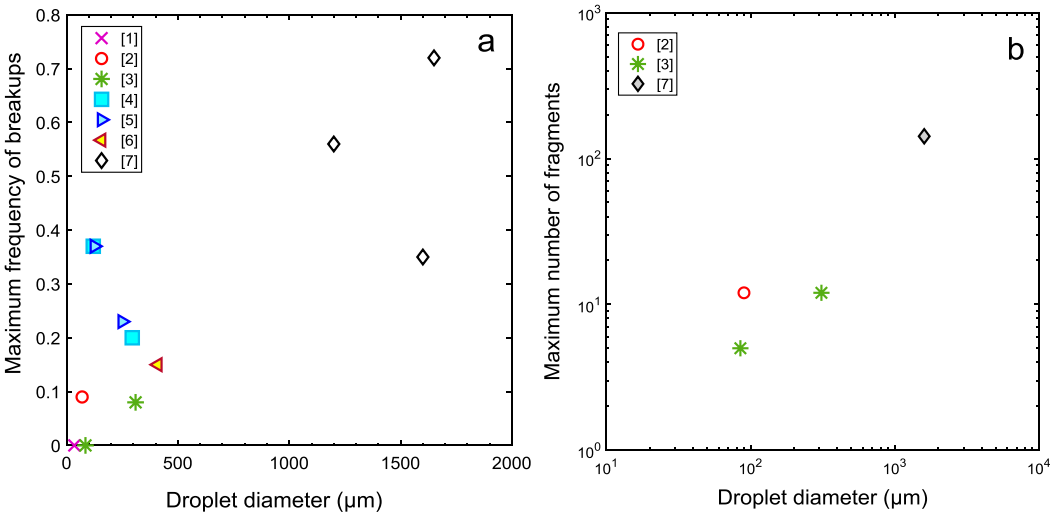

FIG. 9. Previous results of the laboratory studies of SIP. (a) The maximum frequency of breakups and (b) the maximum number of ejected splinters (if provided) over the droplet size for freely levitated pure water droplets. The reference numbers are as follows: 1–Hobbs and Alkezweeny (1968), 2–Brownscombe and Thorndike (1968), –our own results reported herein, 4–Takahashi (1975), 5–Takahashi and Yamashita (1970), 6–Pruppacher and Schlamp (1975), and 7–Kolomeychuk et al. (1975).

with Kolomeychuk et al. (1975), who investigated droplets of sizes between 1.2 and 1.9 mm at a salt concentration of 5.8 mg L^{-1}, we find that salt is effective in reducing pressure buildup in freezing droplets because of the formation of brine channels and inclusions in the ice shell but only at concentrations above about 100 mg L^{-1}. As the typical salt concentration in cloud droplets larger than 300 μm is about 1 mg L^{-1} (cf. Turner 1955), salt content should not play a role in secondary ice formation from freezing drizzle droplets.

It is instructive to compare the shapes of the frozen droplets that we observe in our experiments with the in situ aircraft observations. Several studies (Korolev et al. 2004; Rangno 2008; Stith et al. 2004) have reported images of hemispherical droplet fragments and frozen droplets with bulges and spicules, suggesting that those shapes were originating from freezing of drizzle drops. Lawson et al. (2015) observed frozen droplets with spicules and droplet fragments during the Ice in Clouds Experiment—Tropical (ICE-T). The ICE-T in particular provided a credible support for the drop freezing SIP, as this mechanism could be active outside the range of conditions imposed by the Hallett–Mossop ice multiplication process (Hallett and Mossop 1974). Based on the ICE-T aircraft measurement, Lawson et al. (2015) have used a one-dimensional (1D) model with mixed-phase bin microphysics scheme to identify the number of secondary ice particles needed to explain their observations and arrived at a functional relationship $N_f = 2.5 \times 10^{-11} d^4$, where N_f is the statistical average number of ice fragments per drop and d is drop diameter (μm). Although we cannot confirm a fourth-power dependency on droplets size, the implication of the strong size dependency of N_f is consistent with our observations.

Recent numerical simulations of Sullivan et al. (2018, 2017) have confirmed the general idea that no single SIP process dominates ice multiplication. However, only the noncollisional SIP mechanisms such as those studied in our work have been found to be capable of very rapid ice number multiplication, a feature that could not be reproduced based on the collision breakup and rime-splintering mechanisms. Moreover, the study of Sullivan et al. (2018) has shown that a less steep sigmoidal functional form of $N_f(d)$ is sufficient to reproduce the observed enhancement of ice particle numbers. We thus argue that SIP mechanisms associated with freezing of drizzle droplets with sufficiently broad size distribution may be an important stage on the path of cloud glaciation.

5. Conclusions

We have identified and quantified four distinct processes that can lead to secondary ice particle formation during the freezing of drizzle-size cloud droplets. In general, we find that bubble bursting from spicules and from the surface are more effective secondary ice mechanisms than droplet-splitting processes. We do not observe the shattering of droplets into many large fragments, as it has been recently reported by Wildeman et al. (2017) for millimeter-sized droplets residing on a

cooled glass slide. It remains unclear if this discrepancy is due to the size difference or the difference in rate and directionality of latent heat flow after freezing.

Even if the number of secondary ice particles produced during individual droplet freezing events could only partially be constrained in this study, we find that the average number of secondary ice particles released during freezing is strongly droplet-size dependent and may well exceed unity for droplets larger than about 300 μm. This leaves droplet fragmentation an important secondary ice process effective at temperatures below −10°C in clouds where large drizzle droplets are present. This result confirms earlier suggestions, like a cascading process of SIP being initiated by drizzle-sized droplets, leading to rapid glaciation (Lawson et al. 2015; Sullivan et al. 2018), which is nicely supported by several field studies. Their models could simulate rapid glaciation observed in maritime cumulus clouds with an algorithm that assumes that the number of secondary ice particles ejected upon freezing is a function of the droplet diameter.

Acknowledgments. This work was supported in part by the program ATMO of the Helmholtz Association. We acknowledge fruitful discussions with Andrew Heymsfield, Alexei Korolev, Paul Lawson, Zev Levin, Athanasios Nenes, and Sylvia Sullivan during various stages of this project. We are in debt to two anonymous referees and Arthur Rangno for very helpful reviews of the original manuscript.

REFERENCES

Beheng, K. D., 1987: Microphysical properties of glaciating cumulus clouds: Comparison of measurements with a numerical simulation. *Quart. J. Roy. Meteor. Soc.*, **113**, 1377–1382, https://doi.org/10.1002/qj.49711347815.

Braham, R. R., 1964: What is the role of ice in summer rain-showers? *J. Atmos. Sci.*, **21**, 640–645, https://doi.org/10.1175/1520-0469(1964)021<0640:WITROI>2.0.CO;2.

Brownscombe, J. L., and N. S. C. Thorndike, 1968: Freezing and shattering of water droplets in free fall. *Nature*, **220**, 687–689, https://doi.org/10.1038/220687a0.

Chisnell, R. F., and J. Latham, 1974: A stochastic model of ice particle multiplication by drop splintering. *Quart. J. Roy. Meteor. Soc.*, **100**, 296–308, https://doi.org/10.1002/qj.49710042504.

Crosier, J., and Coauthors, 2011: Observations of ice multiplication in a weakly convective cell embedded in supercooled mid-level stratus. *Atmos. Chem. Phys.*, **11**, 257–273, https://doi.org/10.5194/acp-11-257-2011.

Dye, J. E., W. P. Winn, J. J. Jones, and D. W. Breed, 1989: The electrification of New Mexico thunderstorms: 1. Relationship between precipitation development and the onset of electrification. *J. Geophys. Res.*, **94**, 8643–8656, https://doi.org/10.1029/JD094iD06p08643.

Field, P. R., and Coauthors, 2017: Secondary ice production: Current state of the science and recommendations for the future. *Ice Formation and Evolution in Clouds and Precipitation: Measurement and Modeling Challenges*, *Meteor. Monogr.*, No. 58, Amer. Meteor. Soc., https://doi.org/10.1175/AMSMONOGRAPHS-D-16-0014.1.

Hallett, J., and S. C. Mossop, 1974: Production of secondary ice particles during the riming process. *Nature*, **249**, 26–28, https://doi.org/10.1038/249026a0.

Harris-Hobbs, R. L., and W. A. Cooper, 1987: Field evidence supporting quantitative predictions of secondary ice production rates. *J. Atmos. Sci.*, **44**, 1071–1082, https://doi.org/10.1175/1520-0469(1987)044<1071:FESQPO>2.0.CO;2.

Hobbs, P. V., and A. J. Alkezweeny, 1968: The fragmentation of freezing water droplets in free fall. *J. Atmos. Sci.*, **25**, 881–888, https://doi.org/10.1175/1520-0469(1968)025<0881:TFOFWD>2.0.CO;2.

——, and A. L. Rangno, 1985: Ice particle concentrations in clouds. *J. Atmos. Sci.*, **42**, 2523–2549, https://doi.org/10.1175/1520-0469(1985)042<2523:IPCIC>2.0.CO;2.

——, and ——, 1990: Rapid development of high ice particle concentrations in small polar maritime cumuliform clouds. *J. Atmos. Sci.*, **47**, 2710–2722, https://doi.org/10.1175/1520-0469(1990)047<2710:RDOHIP>2.0.CO;2.

Hoffmann, N., A. Kiselev, D. Rzesanke, D. Duft, and T. Leisner, 2013: Experimental quantification of contact freezing in an electrodynamic balance. *Atmos. Meas. Tech.*, **6**, 2373–2382, https://doi.org/10.5194/amt-6-2373-2013.

Hogan, R. J., P. R. Field, A. J. Illingworth, R. J. Cotton, and T. W. Choularton, 2002: Properties of embedded convection in warm-frontal mixed-phase cloud from aircraft and polarimetric radar. *Quart. J. Roy. Meteor. Soc.*, **128**, 451–476, https://doi.org/10.1256/003590002321042054.

Johnson, D. A., and J. Hallett, 1968: Freezing and shattering of supercooled water drops. *Quart. J. Roy. Meteor. Soc.*, **94**, 468–482, https://doi.org/10.1002/qj.49709440204.

Knight, C. A., and N. C. Knight, 1974: Drop freezing in clouds. *J. Atmos. Sci.*, **31**, 1174–1176, https://doi.org/10.1175/1520-0469(1974)031<1174:DFIC>2.0.CO;2.

Knollenberg, R. G., 1976: Three new instruments for cloud physics measurements: The 2-D spectrometer, the Forward Scattering Spectrometer Probe, and the active scattering aerosol spectrometer. Preprints, *Int. Cloud Physics Conf.*, Boulder, CO, Amer. Meteor. Soc., 554–561.

Koenig, L. R., 1963: The glaciating behavior of small cumulonimbus clouds. *J. Atmos. Sci.*, **20**, 29–47, https://doi.org/10.1175/1520-0469(1963)020<0029:TGBOSC>2.0.CO;2.

Kolomeychuk, R. J., D. C. McKay, and J. V. Iribarne, 1975: The fragmentation and electrification of freezing drops. *J. Atmos. Sci.*, **32**, 974–979, https://doi.org/10.1175/1520-0469(1975)032<0974:TFAEOF>2.0.CO;2.

Korolev, A. V., M. P. Bailey, J. Hallett, and G. A. Isaac, 2004: Laboratory and in situ observation of deposition growth of frozen drops. *J. Appl. Meteor.*, **43**, 612–622, https://doi.org/10.1175/1520-0450(2004)043<0612:LAISOO>2.0.CO;2.

——, E. F. Emery, J. W. Strapp, S. G. Cober, G. A. Isaac, M. Wasey, and D. Marcotte, 2011: Small ice particles in tropospheric clouds: Fact or artifact? Airborne Icing Instrumentation Evaluation Experiment. *Bull. Amer. Meteor. Soc.*, **92**, 967–973, https://doi.org/10.1175/2010BAMS3141.1.

Lawson, R. P., S. Woods, and H. Morrison, 2015: The microphysics of ice and precipitation development in tropical cumulus clouds. *J. Atmos. Sci.*, **72**, 2429–2445, https://doi.org/10.1175/JAS-D-14-0274.1.

MacGorman, D. R., and W. D. Rust, 1998: *The Electrical Nature of Storms.* Oxford University Press, 422 pp.

Mossop, S. C., 1970: Concentrations of ice crystals in clouds. *Bull. Amer. Meteor. Soc.*, **51**, 474–479, https://doi.org/10.1175/1520-0477(1970)051<0474:COICIC>2.0.CO;2.

——, 1985: The origin and concentration of ice crystals in clouds. *Bull. Amer. Meteor. Soc.*, **66**, 264–273, https://doi.org/10.1175/1520-0477(1985)066<0264:TOACOI>2.0.CO;2.

——, R. E. Ruskin, and K. J. Heffernan, 1968: Glaciation of a cumulus at approximately −4C. *J. Atmos. Sci.*, **25**, 889–899, https://doi.org/10.1175/1520-0469(1968)025<0889:GOACAA>2.0.CO;2.

——, A. Ono, and E. R. Wishart, 1970: Ice particles in maritime clouds near Tasmania. *Quart. J. Roy. Meteor. Soc.*, **96**, 487–508, https://doi.org/10.1002/qj.49709640910.

——, R. E. Cottis, and B. M. Bartlett, 1972: Ice crystal concentrations in cumulus and stratocumulus clouds. *Quart. J. Roy. Meteor. Soc.*, **98**, 105–123, https://doi.org/10.1002/qj.49709841509.

Oraltay, R. G., and J. Hallett, 1989: Evaporation and melting of ice crystals: A laboratory study. *Atmos. Res.*, **24**, 169–189, https://doi.org/10.1016/0169-8095(89)90044-6.

Pander, T. J., 2015: Laboratory ice multiplication experiments in levitated microdroplets. Ph.D. dissertation, Heidelberg University, 136 pp.

Petrovic, J. J., 2003: Review: Mechanical properties of ice and snow. *J. Mater. Sci.*, **38**, 1–6, https://doi.org/10.1023/A:1021134128038.

Phillips, V. T. J., T. W. Choularton, A. J. Illingworth, R. J. Hogan, and P. R. Field, 2003: Simulations of the glaciation of a frontal mixed-phase cloud with the explicit microphysics model. *Quart. J. Roy. Meteor. Soc.*, **129**, 1351–1371, https://doi.org/10.1256/qj.02.100.

Pruppacher, H. R., and R. J. Schlamp, 1975: A wind tunnel investigation on ice multiplication by freezing of waterdrops falling at terminal velocity in air. *J. Geophys. Res.*, **80**, 380–386, https://doi.org/10.1029/JC080i003p00380.

——, and J. D. Klett, 1997: *Microphysics of Clouds and Precipitation.* Vol. 18. Kluwer Academic, 954 pp.

Rangno, A. L., 2008: Fragmentation of freezing drops in shallow maritime frontal clouds. *J. Atmos. Sci.*, **65**, 1455–1466, https://doi.org/10.1175/2007JAS2295.1.

——, and P. V. Hobbs, 1991: Ice particle concentrations and precipitation development in small polar maritime cumuliform clouds. *Quart. J. Roy. Meteor. Soc.*, **117**, 207–241, https://doi.org/10.1002/qj.49711749710.

——, and ——, 1994: Ice particle concentrations and precipitation development in small continental cumuliform clouds. *Quart. J. Roy. Meteor. Soc.*, **120**, 573–601, https://doi.org/10.1002/qj.49712051705.

——, and ——, 2001: Ice particles in stratiform clouds in the Arctic and possible mechanisms for the production of high ice concentrations. *J. Geophys. Res.*, **106**, 15 065–15 075, https://doi.org/10.1029/2000JD900286.

Rzesanke, D., J. Nadolny, D. Duft, R. Muller, A. Kiselev, and T. Leisner, 2012: On the role of surface charges for homogeneous freezing of supercooled water microdroplets. *Phys. Chem. Chem. Phys.*, **14**, 9359–9363, https://doi.org/10.1039/c2cp23653b.

Stith, J. L., J. A. Haggerty, A. Heymsfield, and C. A. Grainger, 2004: Microphysical characteristics of tropical updrafts in clean conditions. *J. Appl. Meteor.*, **43**, 779–794, https://doi.org/10.1175/2104.1.

Sullivan, S. C., C. Hoose, and A. Nenes, 2017: Investigating the contribution of secondary ice production to in-cloud ice crystal numbers. *J. Geophys. Res. Atmos.*, **122**, 9391–9412, https://doi.org/10.1002/2017JD026546.

——, ——, A. Kiselev, T. Leisner, and A. Nenes, 2018: Initiation of secondary ice production in clouds. *Atmos. Chem. Phys.*, **18**, 1593–1610, https://doi.org/10.5194/acp-18-1593-2018.

Sun, J., P. A. Ariya, H. G. Leighton, and M. K. Yau, 2010: Mystery of ice multiplication in warm-based precipitating shallow cumulus clouds. *Geophys. Res. Lett.*, **37**, L10802, https://doi.org/10.1029/2010GL042440.

Takahashi, C., 1975: Deformations of frozen water drops and their frequencies. *J. Meteor. Soc. Japan*, **53**, 402–411, https://doi.org/10.2151/jmsj1965.53.6_402.

——, and A. Yamashita, 1970: Shattering of frozen water drops in a supercooled cloud. *J. Meteor. Soc. Japan*, **48**, 373–376, https://doi.org/10.2151/jmsj1965.48.4_373.

Taylor, J. W., and Coauthors, 2016: Observations of cloud microphysics and ice formation during COPE. *Atmos. Chem. Phys.*, **16**, 799–826, https://doi.org/10.5194/acp-16-799-2016.

Turner, J. S., 1955: The salinity of rainfall as a function of drop size. *Quart. J. Roy. Meteor. Soc.*, **81**, 418–429, https://doi.org/10.1002/qj.49708134911.

Vardiman, L., 1978: The generation of secondary ice particles in clouds by crystal–crystal collision. *J. Atmos. Sci.*, **35**, 2168–2180, https://doi.org/10.1175/1520-0469(1978)035<2168:TGOSIP>2.0.CO;2.

Wildeman, S., S. Sterl, C. Sun, and D. Lohse, 2017: Fast dynamics of water droplets freezing from the outside in. *Phys. Rev. Lett.*, **118**, 084101, https://doi.org/10.1103/PhysRevLett.118.084101.

Yano, J.-I., V. T. J. Phillips, and V. Kanawade, 2016: Explosive ice multiplication by mechanical break-up in ice–ice collisions: A dynamical system-based study. *Quart. J. Roy. Meteor. Soc.*, **142**, 867–879, https://doi.org/10.1002/qj.2687.